International Journal of Engineering Research & Management Technology
ISSN: 2348-4039
April-2019 Volume 6, Issue-2
Email:editor@ijermt.org www.ijermt.org

SIMULATION OF BALLISTIC IMPACTS OF ALUMINUM PLATES WITH OGIVE-NOSE STEEL PROJECTILES

Vladimir S. Sokolinsky[1], Juan A. Hurtado[2]
[1]Division of Structural Engineering, Shamoon College of Engineering, Ashdod 77245, Israel
[2]Dassault Systèmes SIMULIA Corp., Providence, RI 02909, USA

ABSTRACT
Accurate numerical simulation of ballistic impact events can provide physical insights into the perforation process that might be beyond experimental ability, shorten the product development cycle, and reduce cost in various industries. The high-velocity perforation process is very complex and requires the use of reliable and robust constitutive models capable of simulating material response at high strain rates, high pressures, and progressive damage. In this paper, a methodology is described for modeling of the ballistic impact of metal projectiles on metal targets in the ordnance velocity range (~0.5–2.0 km/s) using Abaqus/Explicit commercial finite element software. The constitutive models used in the simulations account for the effects of strain, strain rate, temperature, and adiabatic heating on the material behavior. Because material damage develops before the appearance of the penetration and strongly influences its progress, it is accounted for in the analysis for both the target and the projectile. Very good quantitative and qualitative agreement is shown between the numerical results and experimental data for both normal and oblique impacts, demonstrating the capability of Abaqus/Explicit for assessing the projectile residual velocities and time-resolved kinematics and reducing the amount of experimental testing.

KEYWORDS: Aluminum plates; ballistic impact; perforation; progressive damage; Abaqus/Explicit analysis

INTRODUCTION
The inclusion of high-velocity impact dynamics in engineering practice allows analysts to account for the effects of penetrating fragments, accidental loads, and collisions. Moreover, it allows for a more thorough design of lightweight protective structures for civil and military use, whose importance has grown dramatically in recent years.

Depending on the type and velocity of the impacting bodies, their structural response can vary from recoverable elastic deformation to material rupture with local state transitions. When a material is stressed far beyond its elastic limit, shock waves are generated, and such waves are capable of creating a pressure of a magnitude that can significantly exceed the material's strength. In these circumstances, a solid material at the early stages of the event can be considered as a compressible fluid, with strength effects appearing later (Zukas 2004, Hiermaier 2008, Yu and Qiu 2018). Material damage develops before penetration and strongly influences its progress, and thus it should be adequately accounted for in the analysis. A simulation capability for high-velocity impact events must, therefore, employ reliable and robust constitutive models capable of simulating material response at high strain rates, high pressure, and progressive damage.

Corbett (2006) studied normal impacts between 3.175 mm diameter aluminum spherical projectiles and 1.6 mm thick aluminum targets at room and elevated (110 and 210 °C) temperatures. The simulated impact velocities ranged from approximately 2 to7 km/s. The AUTODYN hydro code was used in the numerical study, and the results were compared with empirical data obtained from the literature and the University of Denver Research Institute's two-stage light gas gun experiments. The best correlation between the numerically simulated and the experimentally obtained target hole diameters was found for the models based on the Johnson-Cook strength and failure models for the target and the Johnson-Cook

strength and principal stress failure models for the projectile.

Schwer (2009) used the LS-DYNA Explicit Finite Element Analysis software to simulate normal impacts between a blunt aluminum cylindrical projectile of length 24.7 mm and diameter 16.7 mm and a 12.7 mm thick aluminum plate target. The simulated impact velocity was 970 m/s. Three numerical techniques were used in the simulations: (a) Lagrangian with element erosion; (b) Multi-Material Arbitrary Lagrangian-Eulerian (MM-ALE); and (c) Smooth Particle Hydrodynamics (SPH). The constitutive behavior of both the projectile and the target was represented by the Johnson-Cook material model and the polynomial equation of state for aluminum 6061-T6 suggested by Vahedi and Khazraiyan (2004). The Johnson-Cook failure criterion was used with solid Lagrangian elements to allow for element erosion. The Lagrangian technique showed the best correlation with the experimental residual velocity of the projectile among the three numerical methods used.

Erice *et al.* (2014) conducted an experimental and numerical study of ballistic impacts on precipitation hardened Inconel 718 nickel-base superalloy plates with a thickness of 1.6 mm by spherical steel projectiles with a diameter of 5.55 mm. The initial projectile velocities ranged from 300 m/s to 800 m/s. Because the choice of a target-projectile pair was the imitation of an engine blade-off event in the low-pressure turbine working environment, the ballistic impact tests were carried out at 25 °C, 400 °C, and 700 °C. The elevated temperatures were achieved using a ballistic furnace installed in the impact chamber. The numerical simulation was performed using the LS-Dyna explicit finite element commercial software. The coupled elastoplastic-damage constitutive model with the Johnson-Cook dynamic failure criterion dependent on the third invariant of the stress deviator tensor (Lode angle) was implemented as an LS-Dyna user-defined material subroutine. The authors reported excellent predictions of the residual velocity for high temperatures although those for room temperature were less accurate. The accuracy of the residual velocity prediction was directly dependent on the prediction of adiabatic shear bands and, therefore, on the finite element mesh size.

Kpenyigba *et al*. (2013) and Jankowiak *et al.* (2014) performed an experimental and numerical study of normal impacts and perforations of 1 mm thick mild steel sheets by 13 mm diameter maraging steel hemispherical, conical, and blunt projectiles. The impact velocities ranged from 35 to 180 m/s. The experimental arrangement included a high-speed camera, a gas gun, laser sensors (for the initial velocity measurements), and laser barriers (for the residual velocity measurements). The numerical analysis was conducted using Abaqus/Explicit commercial finite element software. The authors reported good correspondence between the numerical and experimentally observed failure patterns, perforation times, and residual velocities. Also, a good correlation between a theoretically predicted and the simulated average impact force for the hemispherical projectile was demonstrated. In addition, an approximated parabolic description of the variation of the impact force with time was suggested.

Kpenyigba *et al*. (2015) further explored the influence of the projectile shape on the ballistic response of thin mild steel targets subjected to normal impacts by maraging steel hemispherical, conical, and double-nose (a combination of conical and hemispherical shapes) projectiles. The thermo-viscoplastic behavior of the target material was modeled using the Rusinek-Klepaczko (RK) constitutive model, which had been implemented as an Abaqus/Explicit user subroutine. The authors reported a significant dependence of the ballistic limit, the failure mode, and the energy absorption capacity of the target on the projectile nose shape.

Bendarma *et al.* (2017) studied the ballistic response of 1 mm thick 1050 aluminum alloy sheets impacted by 12 mm maraging steel conical projectiles using an experimental and numerical approach similar to that reported in Jankowiak *et al.* (2014) and Kpenyigba *et al*. (2013, 2015). The authors reported a good correlation between numerical and experimental results.

De Vuyst *et al.* (2017) studied, experimentally and numerically, the effect of the orientation of cubical projectiles with an edge length of 9.5 mm on the ballistic limit and failure modes of aluminum alloy

AA2024-T351 sheets with a thickness of 3.175 mm. A single stage gas gun was used to accelerate the projectiles from approximately 198 to 324 m/s. An optical velocity measurement system consisting of two light beams and photodiodes was used for the projectile velocity measurements. The desired projectile orientation at impact was achieved by placing the projectiles in a sabot and reducing the free flight distance to 50 mm. Face, edge, and corner impacts were investigated. The numerical study was performed by using the LS-Dyna explicit finite element commercial software. The lowest and the highest ballistic limits were registered for an edge and corner impacts, respectively, with a difference of 25% between the ballistic limit velocities. The authors concluded that these differences in impact response are caused by the way momentum is transferred from the cubic projectile to the thin target resulting in different failure mechanisms.

Banerjee *et al.* (2017) investigated normal impacts and perforations of 50 mm thick armor steel plates by 40 mm diameter ogive-nosed hardened steel cylindrical projectiles moving with velocities between 550 and 750 m/s. The numerical study was conducted with the aid of Altair Hyper Works commercial finite element package. The Johnson-Cook material and failure models were used to model the response of the target, and the elastic material behavior was assumed to model the hardened steel projectile. The parameters of Johnson-Cook constitutive relation and the failure model for armor steel material used in the study were reported in the experimental work by the same authors (Banerjee *et al.* 2014). Good agreement between the calculated and experimental ballistic limit velocities and reliable simulation of the perforation process was reported.

The Abaqus/Explicit simulations presented here examine the perforation of 26.3 mm thick aluminum plate specimens impacted with 3.0 caliber-radius-head ogive-nose steel rods. The constitutive models used in the simulations account for the effects of strain, strain rate, temperature, and progressive damage on the material behavior that permits to simulate the complex phenomenon of interaction between the deformations of the projectile and the target. The geometry and material properties of the steel rods (projectiles) and aluminum plates (targets) were taken from Piekutowski *et al.* (1996).

ANALYSIS APPROACH

The projectile is an ogive-nose rod with the 3.0 caliber-radius-head machined from 4340 $R_c = 44$ steel rod stock (see Fig. 1). The Young's modulus and the 0.2% offset yield strength of the material are 202 GPa and 1,430 MPa, respectively. The projectile's mass is approximately 81gram. The target is a 304 mm square plate cut from a single 6061-T651 aluminum plate of thickness 26.3 mm. The Young's modulus and the 0.2% offset yield strength of the material are 69 GPa and 262 MPa, respectively. Experiments in Piekutowski *et al*. (1996) showed this material to be practically rate independent. The results of the numerical simulations were compared with measured residual velocities and the X-ray photographs of the perforation process in Piekutowski *et al*. (1996).

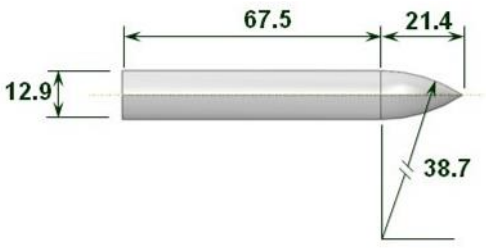

Fig. 1 Schematic of the projectile (dimensions in millimeters)

The finite element models for normal and oblique impacts were created in the Abaqus preprocessing and visualization environment Abaqus/CAE. In the latter case, the angle between the projectile velocity vector and the plate normal is 30° (see Fig. 2). As noted in Zukas (1993), the accuracy of any impact simulation strongly depends on (a) the mesh; (b) the constitutive model; and (c) the data used in the material model. These important simulation factors are discussed further.

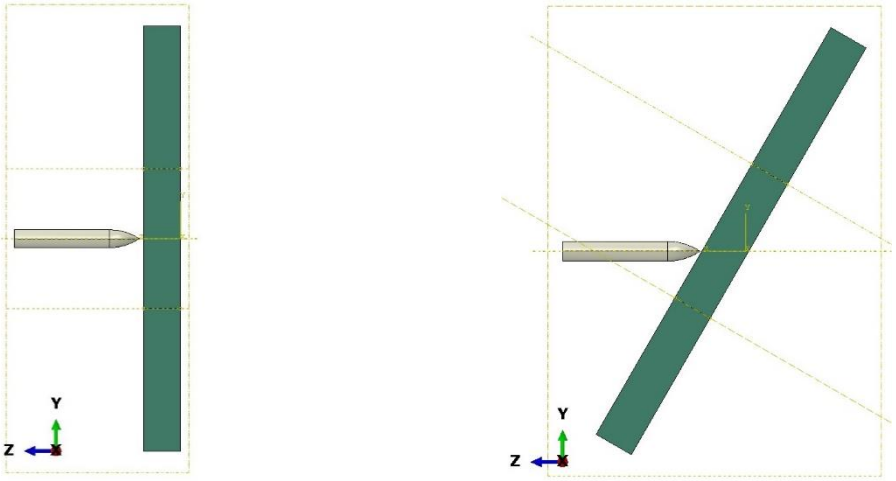

(a) Normal impact (b) Oblique impact

Fig. 2 Abaqus/CAE impact models

MESH DETAILS

An eight-node brick element with reduced integration (C3D8R) was used to build the model. A mesh size convergence study required 12 elements along the projectile diameter and 26 elements through the target thickness, which resulted in a practically uniform mesh with an element edge of 1 mm. The resulting finite element model had approximately 7.5 million degrees of freedom and permitted to capture the complex phenomenon of interaction between the deformations of the relatively thick projectile and the target.

CONSTITUTIVE MODEL

When the pressure generated by shock wave propagation exceeds the material strength by several orders of magnitude, the early stages of material response can be regarded as hydrodynamic; strength effects appear in the late stages of the event Zukas (2004). Therefore, it is assumed for both metal materials that volumetric behavior is described by the Mie-Grüneisen equation of state (EOS) model, with the deviatoric behavior described by the linear elastic and the Johnson-Cook plasticity models. Note that the Mie-Grüneisen form of the EOS model is suitable only for solids and, therefore, cannot be used in simulations with impact velocities larger than 2 km/s, where solid-liquid-gas transitions occur in the material.

The Mie-Grüneisen equation of state model is given by (Nagayama 2011, Simulia 2012)

$$\begin{aligned} p &= p_H\left(1-\frac{\Gamma_0\eta}{2}\right)+\Gamma_0\rho_0 E_m \\ p_H &= \frac{\rho_0 c_0^2\eta}{(1-s\eta)^2} \\ \eta &= 1-\frac{\rho_0}{\rho}, \end{aligned} \qquad (1)$$

where p is the pressure stress (defined as positive in compression), p_H is the Hugoniot pressure, Γ_0 is the Grüneisen coefficient, η is the nominal volumetric compressive strain, ρ_0 is the reference density, ρ is the current density, and E_m is the internal energy per unit mass. The parameters c_0 and s define the linear relationship between the linear shock velocity, U_s, and the particle velocity, U_p, as follows (the so-called linear U_s–U_p Hugoniot form):

$$U_s = c_0 + sU_p. \qquad (2)$$

The EOS model in Eq. (1) requires the input of the: (a) reference density, ρ_0; (b) Grüneisen coefficient,

Γ_0; and (c) parameters c_0 and s. The values of these parameters used in the present analysis were taken from Steinberg (1996) and Corbett (2006) and are given in Table 1. Because it is not always possible to find the data for the required material, the parameter values in the table correspond to the materials with mechanical properties close to those used for the aluminum target and steel projectile. Providing the value of the specific heat allows for modeling the adiabatic heating of a material due to plastic dissipation through the analysis.

Table 1 Input parameters for the Mie-Grüneisen EOS model

Material	Reference density, ρ_0 (g/cm^3)	Grüneisen coefficient, Γ_0	Parameter c_0 (cm/μs)	Parameter s	Reference temperature (K)	Specific heat (J/(kg K))
Aluminum 6061-T6	2.703	1.97	0.524	1.40	293.2	885.0
Steel 4340, $R_c = 38$	7.83	1.67	0.4578	1.33	293.2	477.0

The Johnson-Cook model is an incremental elastic-plastic empirical rate model that accounts for strain rate and thermal effects in the material and its compressibility. Johnson-Cook hardening is a particular type of isotropic hardening where the static yield stress, σ^0, is assumed as (Johnson *et al.* 1985, Jones 2012, Simulia 2012):

$$\sigma^0 = \left[A + B\left(\bar{\varepsilon}^{pl}\right)^n\right]\left(1 - \hat{\theta}^m\right), \tag{3}$$

where $\bar{\varepsilon}^{pl}$ is the equivalent plastic strain; A, B, n, and m represent the yield stress, hardening constant, hardening exponent, and thermal softening exponent, respectively; and $\hat{\theta}$ is the nondimensional temperature which is defined in terms of the current temperature, θ, the melting temperature, θ_{melt}, and the transition temperature, $\theta_{transition}$, as follows

$$\hat{\theta} = \begin{cases} 0 & \text{for } \theta < \theta_{transition} \\ \dfrac{\theta - \theta_{transition}}{\theta_{melt} - \theta_{transition}} & \text{for } \theta_{transition} \le \theta \le \theta_{melt} \\ 1 & \text{for } \theta > \theta_{melt} \ . \end{cases} \tag{4}$$

Johnson-Cook strain rate dependence is given by

$$\bar{\sigma} = \sigma^0\left(\bar{\varepsilon}^{pl}, \theta\right)\left[1 + C \ln\frac{\dot{\bar{\varepsilon}}^{pl}}{\dot{\varepsilon}_0}\right], \tag{5}$$

Where $\bar{\sigma}$ is the yield stress at nonzero strain rate; $\sigma^0(\bar{\varepsilon}^{pl}, \theta)$ is the static yield stress of Eq. (3); $\dot{\bar{\varepsilon}}^{pl}$ is the equivalent plastic strain rate; $\dot{\varepsilon}_0$ and C are material parameters measured at or below the transition temperature.

The values of the parameters in Eqs. (3)-(5) for the materials with mechanical properties close to those used for the aluminum target and steel projectile were taken from Corbett (2006), Johnson and Cook (1985), and Schwer (2009) and are provided in Table 2. These parameters are provided to Abaqus/Explicit as part of the metal plasticity material definition to model plastic hardening and rate dependence.

Table 2 Input parameters for the Johnson-Cook plasticity model

Material	A (MPa)	B (MPa)	n	θ_{melt} (K)	$\theta_{transition}$ (K)	m	C	$\dot{\varepsilon}_0(1/s)$
Aluminum 6061-T6	324.1	113.8	0.42	925	293.2	1.34	0.002	1.0
Steel 4340, C-30	792	510	0.26	1793	293.2	1.03	0.014	1.0

A comparison of the magnitudes of the yield stress, A, in Table 2 with those given previously for the target and projectile shows that the input parameters for the Johnson-Cook model should be calibrated before they can be used in the analysis. Using the true stress-strain experimental data for the aluminum target and steel projectile from Piekutowski *et al.* (1996), A, B, and n for both materials were calibrated so that a close fit between the experimental and numerical true stress-strain curves was achieved. The calibration procedure was performed using MATLAB software. The calibrated input parameters used in the present analysis are given in Table 3. Note that the values of the parameters describing rate-dependency for the aluminum target were not used in the present analysis because, as was mentioned previously, physical experiments showed that the material is practically rate independent.

Table 3 Calibrated input parameters for the Johnson-Cook plasticity model

Material	A (MPa)	B (MPa)	n	θ_{melt} (K)	$\theta_{transition}$ (K)	m	C	$\dot{\varepsilon}_0(1/s)$
Target	262	162.1	0.2783	925	293.2	1.34	–	–
Projectile	1430	2545	0.7	1793	293.2	1.03	0.014	15.0

FAILURE MODEL

The Johnson-Cook dynamic failure model is used as a specific case of the Abaqus ductile damage initiation criterion for metals (Simulia 2012). The ductile criterion is a phenomenological model for predicting the onset of damage due to nucleation, growth, and coalescence of voids. The criterion for damage initiation is met when the damage parameter, ω_D, exceeds 1, i.e.,

$$\omega_D = \int \frac{d\bar{\varepsilon}^{pl}}{\bar{\varepsilon}_D^{pl}\left(\eta, \dot{\bar{\varepsilon}}^{pl}\right)} > 1 \tag{6}$$

where $\bar{\varepsilon}_D^{pl}\left(\eta, \dot{\bar{\varepsilon}}^{pl}\right)$ is the strain at failure, with the summation performed over all increments in the analysis.

When using the Johnson-Cook failure criterion, it is assumed that:

$$\bar{\varepsilon}_D^{pl} = [d_1 + d_2 e^{-d_3\eta}]\left[1 + d_4 \ln\left(\frac{\dot{\bar{\varepsilon}}^{pl}}{\dot{\varepsilon}_0}\right)\right]\left(1 + d_5\hat{\theta}\right) \tag{7}$$

where failure parameters $d_1 - d_5$ are measured at or below the transition temperature, $\theta_{transition}$, and $\dot{\varepsilon}_0$ is the reference strain rate (see also Eq. (5)). The values of the failure parameters should be provided when using the Johnson-Cook dynamic failure model in Abaqus/Explicit.

The Johnson-Cook failure parameters that were used in the present analysis for the aluminum target and steel projectile were taken from Corbett (2006), Johnson and Cook (1985), and Schwer (2009) and are shown in Table 4.

Table 4 Input parameters for the Johnson-Cook dynamic failure model

Material	d_1	d_2	d_3	d_4	d_5
Aluminum 6061-T6	-0.77	1.45	0.47	0.0	1.6
Steel 4340, C-30	0.05	3.44	2.12	0.002	0.61

It is important to note that the failure parameter d_3 is reported as being a negative number for a specific material in the literature. However, as explained in the documentation, Abaqus implementation of a Johnson-Cook general expression for the strain at fracture expects this parameter being positive. Failure to properly account for the sign of d_3 will lead to an incorrect response. Besides the values of the failure parameters, the values of the melting (θ_{melt}) and transition ($\theta_{transition}$) temperatures and the reference strain rate ($\dot{\varepsilon}_0$) are required for a complete description of the initiation criterion. Clearly, the temperature values should be consistent with those used for the plasticity definition as given in Table 3.

Choosing a zero value for the fracture energy, which is used as a data parameter for the damage evolution law, completes the settings of the failure model. Elements are deleted by default upon reaching maximum degradation according to the usual rules of the Abaqus progressive damage framework.

INITIAL AND BOUNDARY CONDITIONS

The target was clamped along its perimeter, and an initial velocity was prescribed to the projectile. Due to high sliding velocities, frictionless contact was assumed between the target and projectile. Also, initial room temperatures (293.2 K) were prescribed for both the target and projectile. The hourglass stiffness was scaled by 50 times for the normal impact simulations and 15 times for the oblique impact simulations to preserve the projectile's nose from deformations and damage as observed in the experiments.

RESULTS

NORMAL IMPACT

Close agreement between the experimental (Piekutowski *et al.* 1996) and simulated residual velocities for a range of striking velocities can be seen from Fig. 3. The maximum deviation of 5.6 percent is obtained for the lowest striking velocity, and for the highest velocity, the deviation reduces to only 1.6 percent. Fig. 4 illustrates the perforation process for each striking velocity presented in Fig. 3 at the time instances for which the X-ray photographs were made in Piekutowski *et al.* (1996). The results shown in Fig. 4 are in close agreement with the time-resolved projectile kinematics in Piekutowski *et al.* (1996). Note specifically that the projectile remains undeformed, which fully corresponds to the experimental evidence.

OBLIQUE IMPACT

The experimental (Piekutowski *et al.* 1996) and simulated residual velocities for a range of striking velocities are compared in Fig. 5. As can be seen from the figure, the numerical and experimental results for lower striking velocities are further apart than for the normal impact; but, in general, the agreement between the simulation and experiment is good. Analogously to the normal impact case, the maximum deviation of 9.7 percent is obtained for the lowest impact velocity, whereas for the highest velocity it practically vanishes. Fig. 6 shows the perforation process for each striking velocity presented in Fig. 5 at the time instances for which the X-ray photographs were made in Piekutowski *et al.* (1996).

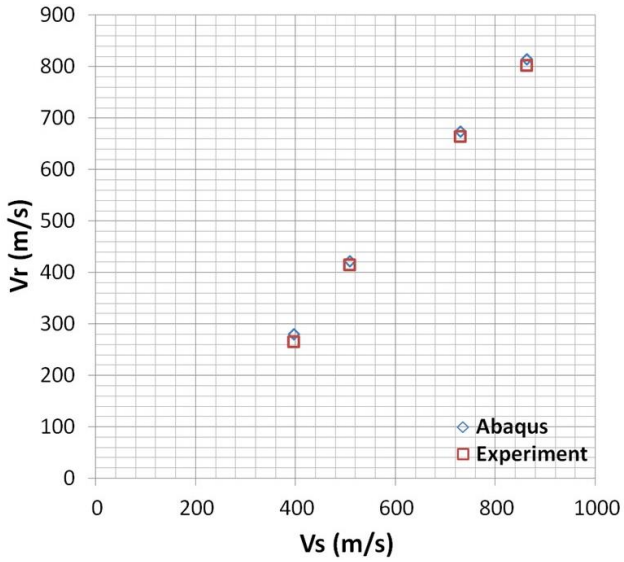

Fig. 3 Experimental and predicted residual (V_r) vs. striking (V_s) velocities for normal impact

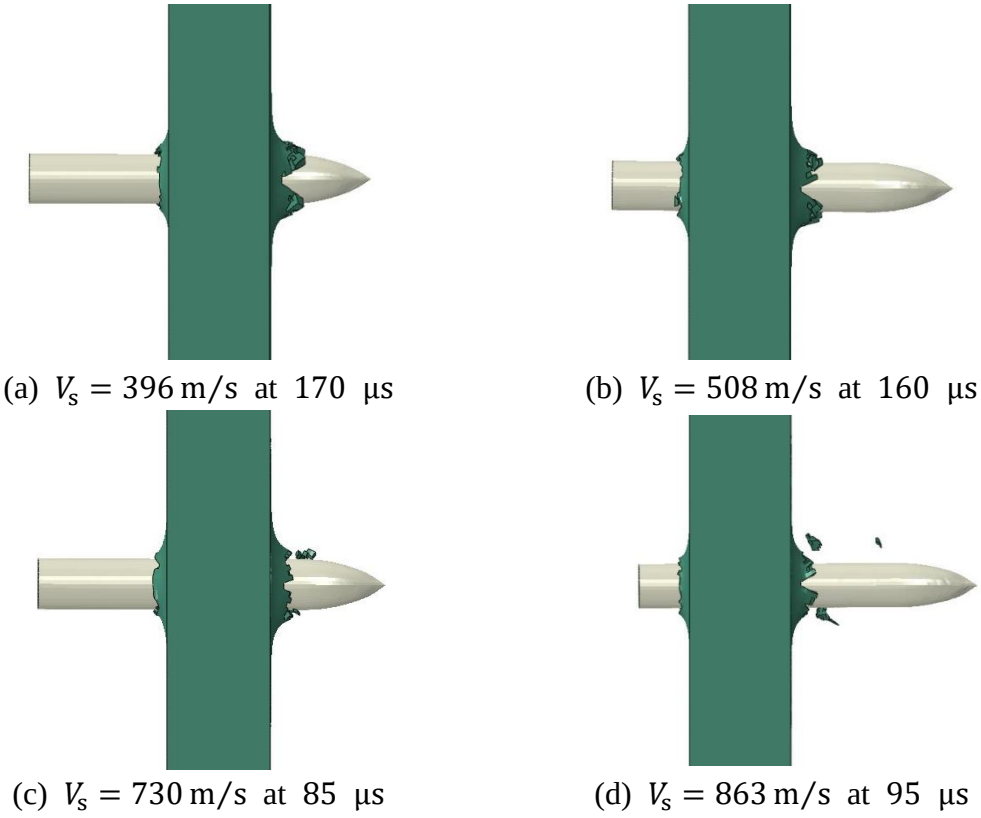

(a) $V_s = 396\,\mathrm{m/s}$ at 170 μs (b) $V_s = 508\,\mathrm{m/s}$ at 160 μs

(c) $V_s = 730\,\mathrm{m/s}$ at 85 μs (d) $V_s = 863\,\mathrm{m/s}$ at 95 μs

Fig. 4 Perforation process at various velocities and time instances

The results shown in Fig. 6 are in a close agreement with the time-resolved projectile kinematics in Piekutowski *et al.* (1996). Moreover, it can be seen from the figure that the ogive nose remains undeformed, whereas the shank of the projectile exhibits visible bending, which is in accordance with the experimental evidence.

CONCLUSIONS

A methodology for modeling of the ballistic impact of metal projectiles on metal targets in the ordnance velocity range (~0.5–2.0 km/s) using Abaqus/Explicit has been presented. The presented approach permits to simulate the complex phenomenon of interaction between the deformations of the projectile and the target. The simulation results of the ballistic perforation of aluminum plate specimens with ogive-

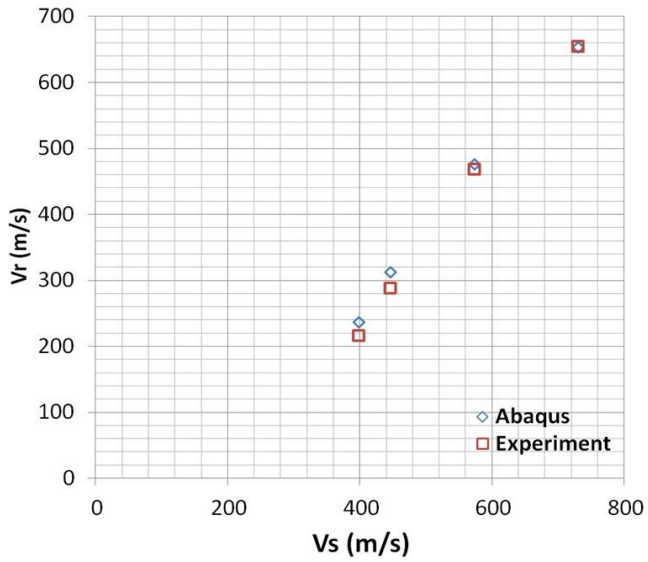

Fig. 5 Experimental and predicted residual (V_r) vs. striking (V_s) velocities for oblique impact

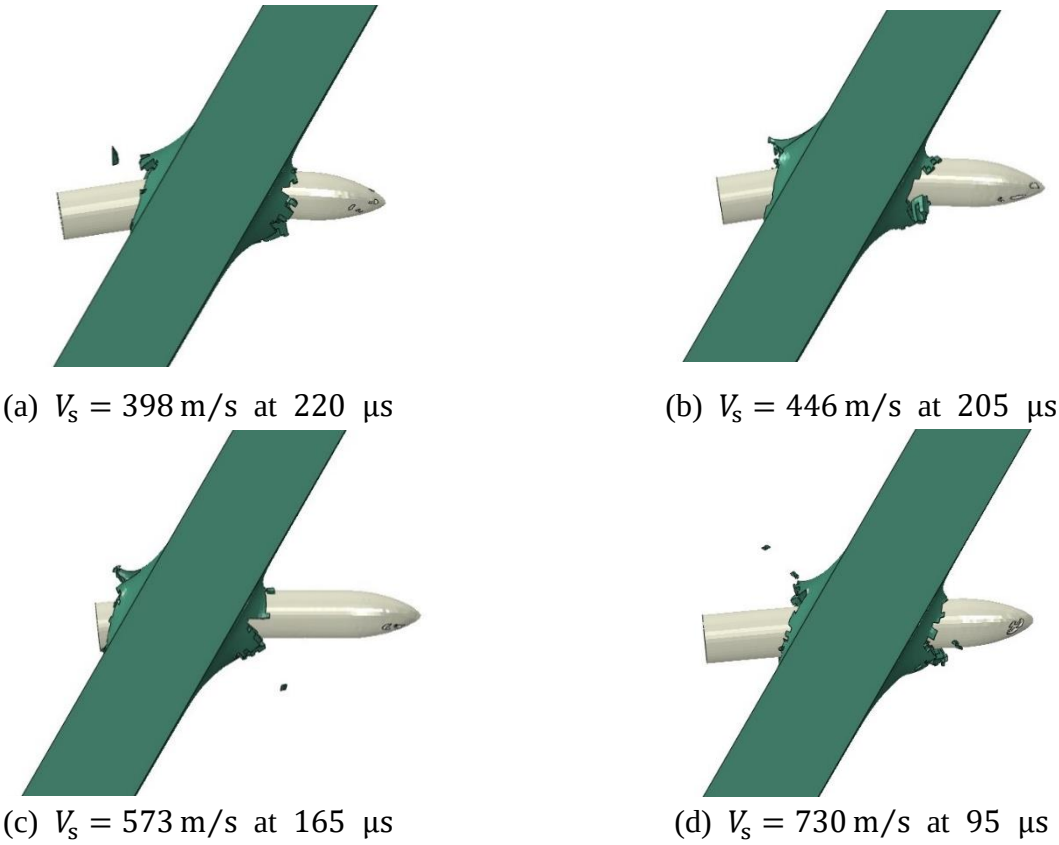

(a) $V_s = 398\,\mathrm{m/s}$ at 220 μs (b) $V_s = 446\,\mathrm{m/s}$ at 205 μs

(c) $V_s = 573\,\mathrm{m/s}$ at 165 μs (d) $V_s = 730\,\mathrm{m/s}$ at 95 μs

Fig. 6 Perforation process at various velocities and time instances

nose steel rods show very good quantitative and qualitative agreement with experimental data for both normal and oblique impacts. The described methodology may thus be used to reduce costly experimental ballistic testing.

ACKNOWLEDGMENTS
The first author would like to express his sincere gratitude to Binoj Ramesh and Fernando Carranza of SIMULIA whose technical advice enhanced the quality of the present work.

REFERENCES

1. Banerjee, A., Dhar, S., Acharyya, S., Datta, D. and Nayak, N. (2014), "An experimental determination of Johnson Cook material and failure model constants for armour steel", *Appl. Mech. Mater*., **592-594**, 990-995.
2. Banerjee, A., Dhar, S., Acharyya, S., Datta, D. and Nayak, N. (2017), "Numerical simulation of ballistic impact of armour steel plate by typical armour piercing projectile", *Procedia Eng*., **173**, 347-354.
3. Bendarma, A., Jankowiak, T., Rusinek, A., Lodygowski, T., Klósak, M. and Bouslikhane, S. (2017), "Perforation analysis of the aluminum alloy sheets subjected to high rate of loading and heated using thermal chamber: experimental and numerical approach", *IJMME*, **11**(4), 334-338.
4. Corbett, B.M. (2006), "Numerical simulations of target hole diameters for hypervelocity impacts into elevated and room temperature bumpers", *Int. J. Impact Eng.*, **33**(1), 431-440.
5. De Vuyst, T., Vignjevic, R., Azorin Albero, A., Hughes, K., Campbell, J.C. and Djordjevic, N. (2017), "The effect of the orientation of cubical projectiles on the ballistic limit and failure mode of AA2024-T351 sheets", *Int. J. Impact Eng.*, **104**, 21-37.
6. Erice, B., Pérez-Martín, M.J. and Galvez, F. (2014), "An experimental and numerical study of ductile failure under quasi-static and impact loadings of Inconel 718 nickel-base superalloy", *Int. J. Impact Eng.*, **69**(2), 11-24.
7. Hiermaier, S.J. (2008), *Structures under Crash and Impact. Continuum Mechanics, Discretization and Experimental Characterization*, Springer Science+Business Media, LLC, New York, NY, USA.
8. Jankowiak, T., Rusinek, A., Kpenyigba, K. M. and Pesci, R. (2014), "Ballistic behavior of steel sheet subjected to impact and perforation", *Steel and Composite Structures*, **16**(6), 595-609.
9. Johnson, G.R. and Cook, W.H. (1985), "Fracture characteristics of three metals subjected to various strains, strain rates, temperatures and pressures", *Eng. Fract. Mech.*, **21**(1), 31-48.
10. Jones, N. (2012), *Structural Impact*, Cambridge University Press, New York, NY, USA
11. Kpenyigba, K.M., Jankowiak, T., Rusinek, A. and Pesci, R. (2013), "Influence of projectile shape on dynamic behavior of steel sheet subjected to impact and perforation", *Thin-Wall. Struct.*, **65**, 93-104.
12. Kpenyigba, K.M., Jankowiak, T., Rusinek, A., Pesci, R. and Wang, B. (2015), "Effect of projectile nose shape on ballistic resistance of interstitial-free steel sheets", *Int. J. Impact Eng.*, **79**, 83-94.
13. Liu, J., Long, Y. and Ji, C. (2018),"Ballistic performance study on the finite steel target subjected to normal and oblique impact by copper explosively formed projectile", *International Journal of Protective Structures*, **9**(4), 461-483.
14. MATLAB 7.11.0, Copyright 1984-2018 The MathWorks, Inc.
15. Nagayama, K. (2011), *Introduction to the Grüneisen Equation of State and Shock Thermodynamics*, First Kindle Edition.
16. Schwer, L. (2009), "Aluminum plate perforation: a comparative study using Lagrange with erosion, multi-material ALE, and smooth particle hydrodynamics", *Proceedings of 7th European LS-DYNA Conference*, Salzburg, Austria, May.
17. Simulia (2012), *Abaqus Analysis User's Manual*, Dassault Systèmes, Providence, RI.
18. Steinberg, D.J. (1996), *Equation of State and Strength Properties of Selected Materials*, Lawrence Livermore National Laboratory, February 13, 1996.
19. Piekutowski, A.J., Forrestal, M.J., Poormon, K.L. and Warren, T.L. (1996), "Perforation of aluminum plates with ogive-nose steel rods at normal and oblique impacts", *Int. J. Impact Eng.*, **18**(7-8), 877-887.
20. Vahedi, Kh. and Khazraiyan, N. (2004), "Numerical modeling of ballistic penetration of long rods into ceramic/metal armor", *Proceedings of 8th International LS-DYNA Users Conference*, Dearborn MI, May.
21. Yu, T.X. and Qiu, X. (2018), *Introduction to Impact Dynamics*, John Wiley & Sons Singapore Pte. Ltd.
22. Zukas, J.A. (1993), "Some common problems in the numerical modeling of impact phenomena", *Comput. Syst. Eng.*, **4**(1), 43-58.
23. Zukas, J.A. (2004), *Introduction to Hydrocodes*, Elsevier, Kidlington, Oxford, UK.